Signatures of site-specific reaction of H-2 on Cu(100)

Somers, M.F.; McCormack, D.A.; Kroes, G.; Olsen, R.A.; Baerends, E.J.; Mowrey, R.C.

published in
Journal of Chemical Physics
2002

DOI (link to publisher)
10.1063/1.1506141

document version
Publisher's PDF, also known as Version of record

Signatures of site-specific reaction of H_2 on Cu(100)

M. F. Somers
Leiden Institute of Chemistry, Gorlaeus Laboratories, Leiden University, P.O. Box 9502, 2300 RA Leiden, The Netherlands

D. A. McCormack
Theoretical Chemistry, Free University, De Boelelaan 1083, 1081 HV Amsterdam, The Netherlands

G. J. Kroes
Leiden Institute of Chemistry, Gorlaeus Laboratories, Leiden University, P.O. Box 9502, 2300 RA Leiden, The Netherlands

R. A. Olsen and E. J. Baerends
Theoretical Chemistry, Free University, De Boelelaan 1083, 1081 HV Amsterdam, The Netherlands

R. C. Mowrey
Theoretical Chemistry Section, Code 6189, Naval Research Laboratory, Washington DC 20375-5342

(Received 30 April 2002; accepted 18 July 2002)

Six-dimensional quantum dynamical calculations are presented for the reaction of $(v,j)\,H_2$ on Cu(100), at normal incidence, for $v=0-1$ and $j=0-5$. The dynamical calculations employed a potential energy surface computed with density functional theory, using the generalized gradient approximation and a slab representation for the adsorbate-substrate system. The aim of the calculations was to establish signatures from which experiments could determine the dominant reaction site of H_2 on the surface and the dependence of the reaction site on the initial rovibrational state of H_2. Two types of signatures were found. First, we predict that, at energies near threshold, the reaction of $(v=1)\,H_2$ is rotationally enhanced, because it takes place at the top site, which has an especially late barrier and a reaction path with a high curvature. On the other hand, we predict the reaction to be almost independent of j for $(v=0)\,H_2$, which reacts at the bridge site. Second, we predict that, at collision energies slightly above threshold for which the reaction probabilities of the $(v=0)$ and $(v=1)$ states are comparable, the rotational quadrupole alignment of $(v=1)$ reacting molecules should be larger than that of $(v=0)$ reacting molecules, for $j=1$, 4, and 5. For $(j=2)\,H_2$, the opposite should be true, and for $(j=3)\,H_2$, the rotational quadrupole alignment should be approximately equal for $(v=1)$ and $(v=0)\,H_2$. These differences can all be explained by the difference in the predicted reaction site for $(v=1)$ and $(v=0)\,H_2$ (top and bridge) and by the differences in the anisotropy of the potential at the reaction barrier geometries associated with these sites. Our predictions can be tested in associative desorption experiments, using currently available experimental techniques. © *2002 American Institute of Physics.* [DOI: 10.1063/1.1506141]

I. INTRODUCTION

The dissociation of H_2 on Cu is a benchmark system for activated surface reactions[1] and has been labeled a ''springboard for new ideas on molecule–surface reactions.''[2] Many experimental[3–24] and theoretical[24–56] studies have been performed on this system, but much remains to be learned.

In the past two decades, progress in the unraveling of H_2+metal–surface reactions has been enormous both for theory[24–73] and experiments.[3–24] Molecular-beam experiments yield reaction probabilities[11,12,21] and inelastic scattering probabilities[17,18,24] that are resolved with respect to the collision energy. With the use of stimulated Raman pumping in molecular-beam experiments, the scattering of H_2 from a specified initial $(v=1,j)$ level can now be investigated for reactive surfaces.[17,18,24] Invoking detailed balance, relative reaction probabilities can be obtained from associative desorption experiments.[12,22,23] Using state-selective detection in combination with time-of-flight techniques, such experiments[12] can now determine energy-resolved relative reaction probabilities which are initial-state selected with respect to both the vibrational state (v) and rotational level (j). Associative desorption experiments can also determine the influence on reaction of the molecule's alignment with respect to the surface by measuring the rotational quadrupole alignment $A_0^{(2)}(v,j)$ of the angular momentum of the desorbing molecules.[13–16]

Theory can now also make important contributions. Reduced-dimensionality theoretical studies on similar systems and models[25,34,37–39,42–52,55–58,69,72] have revealed interesting effects like the vibrational enhancement of the reaction,[40,41,46,52] the effect on the reaction of the corrugation of the potential energy surface (PES),[47] and the effects of the alignment of the incident H_2 molecule.[34,39,42–44,47,48] These calculations and classical trajectory studies[74,75] suggested that in order to obtain quantitatively accurate reaction probabilities, a six-dimensional (6D) quantum study would be needed. This was confirmed in one of the first 6D quantum

studies.[31] In such 6D calculations, the motion in all six degrees of freedom of the incident molecule is modeled without approximation.

Thanks to the improved accuracy of density functional theory[76,77] (DFT) for determining potential energy surfaces (PESs) for H_2+metal systems,[26,78–80] 6D quantum dynamical calculations now yield quantitatively accurate results[26,67,81–83] and are starting to offer a structured procedure for obtaining predictions for experiments.[26,35,59,66,83] In one case, the calculations[66] actually challenged the results of older experiments,[8,10] with newer experiments confirming the validity of the theoretical results.[59] Although 6D calculations have been performed for H_2+Pd(100) (Refs. 60–67), using a time-independent method, and for H_2+Cu(100) (Refs. 26, 28–31, and 35) and H_2+Cu(111) (Refs. 32 and 33), using time-dependent methods, 6D quantum dynamical calculations still represent a formidable task, requiring the use of super computers and specialized codes.

In recent 6D quantum dynamical studies of the H_2+Cu(100) system, a new flux-based method was used to obtain site-specific reaction probabilities for a range of initial rovibrational states of H_2 ($v=0,1$, $j=0,1,4$, with $m_j=0-j$).[26,27] These studies showed that for low incidence energies the reaction does not always occur at the site with the minimum barrier height. Depending on the initial rovibrational state of the H_2 molecule, the dissociation can take place almost exclusively on sites with higher barriers, with total reaction probabilities of the order of 5%. Furthermore, both studies also suggested an experimental signature of the dependence of the preferred reaction site on the initial vibrational state of the molecule. Specifically, it was noted that the rotational quadrupole alignment $A_0^{(2)}(E;v,j)$ of ($v=1$, $j=4$) H_2 should be fairly high compared to the alignment of ($v=0, j=4$) H_2 at low translational energies where the total reaction probability is around 5%. The measurement of this effect would confirm our prediction and therefore support our finding that ($v=1$) H_2 reacts at the top site and ($v=0$) H_2 at the bridge site.[26,27]

The aims of the present study are to see whether the alignment signature for the reaction site previously found for ($j=4$) also holds for other low j values and to find additional signatures for the site-specific reaction. To achieve these goals, calculations were performed on the scattering of (v,j,m_j) H_2 from Cu(100) for $v=0-1$ and $j=0-5$. Our calculations will show that the alignment signature previously found for ($j=4$) H_2 also holds for ($j=1$) and ($j=5$) H_2, but that the differences between the rotational quadrupole alignment of ($v=1$) and ($v=0$) reacting H_2 are related to the preferred reaction sites of ($v=1$) and ($v=0$) H_2 in a different way for ($j=2$) and ($j=3$). We will show that the trends in the alignment of the reacting molecules can be explained by steric hindering effects and an inelastic rotational enhancement effect, in which the molecule transfers energy from its rotation to motion along the reaction path via a rotationally inelastic mechanism.

Our calculations will also show a second signature for the site-specific reaction. This is related to the j dependence of the degeneracy-averaged reaction probabilities, which differs for ($v=1$) and ($v=0$) H_2. We will show that another rotational enhancement mechanism (elastic rotational enhancement, in which the energy transfer from rotation to motion along the reaction path occurs because the molecule's rotational constant is lower at the barrier than in the gas phase) is largely responsible for this.

Section II discusses the system and the dynamical methods we use. In Sec. III the PES is discussed and computational details are given in Sec. IV. Degeneracy-averaged and site-specific degeneracy-averaged reaction probabilities will be presented and discussed in Sec. V A. The question of whether the previously found rotational quadrupole alignment signature holds for all low j ($j=1-5$) will be discussed in Sec. V B. Results for the two experimental signatures found are summarized in Sec. VI.

II. DYNAMICAL METHOD

A. Model

The results of this study are based on a 6D symmetry-adapted close-coupling time-dependent wave packet (SAWP) method.[31] In this method, all degrees of freedom of the H_2 molecule are treated quantum mechanically using two approximations: the Born–Oppenheimer approximation and neglect of phonons.

The use of the Born–Oppenheimer approximation corresponds to the neglect of electron-hole pair excitations and the use of a single PES, in this case the electronic ground state. The validity of this approximation is discussed in Refs. 1, 53, and 84. The neglect of phonons of the Cu(100) surface entails the use of a dynamical model in which the copper atoms are fixed at their ideal lattice positions so that the system, which is in principle of infinite dimensionality, reduces to a 6D problem. Due to the large difference in mass of the hydrogen and copper atoms, the neglect of phonon excitation is thought to be reasonable.[85–87] A more detailed justification of these approximations is given elsewhere.[1,53]

B. Wave packet method

Within the Born–Oppenheimer approximation and the static representation of the metal surface, the Hamiltonian of the system can be written in atomic units:

$$\hat{H}_{6D}=-\frac{1}{2M}\left(\frac{\partial^2}{\partial X^2}+\frac{\partial^2}{\partial Y^2}+\frac{\partial^2}{\partial Z^2}\right)-\frac{1}{2\mu}\frac{\partial^2}{\partial r^2}+\frac{\hat{j}^2}{2\mu r^2}+V(Z,X,Y,r,\theta,\phi). \quad (1)$$

Here X, Y, and Z describe the motion of the center of mass of H_2 and M and μ are the total and reduced masses of the H_2 molecule, respectively. Furthermore, $V(Z,X,Y,r,\theta,\phi)$ is the 6D PES, which depends on the distance of the molecule to the surface, Z; the molecule's center-of-mass coordinates for motion along the surface, X and Y; the H–H distance r; and the angles representing the orientation of the molecule, θ and ϕ (see Fig. 1).

When considering normal incidence only, the symmetry of the metal surface can be used to reduce the computational costs.[31,68,73] The nonsymmetry-adapted wave function can be projected onto a symmetry-adapted basis set, with func-

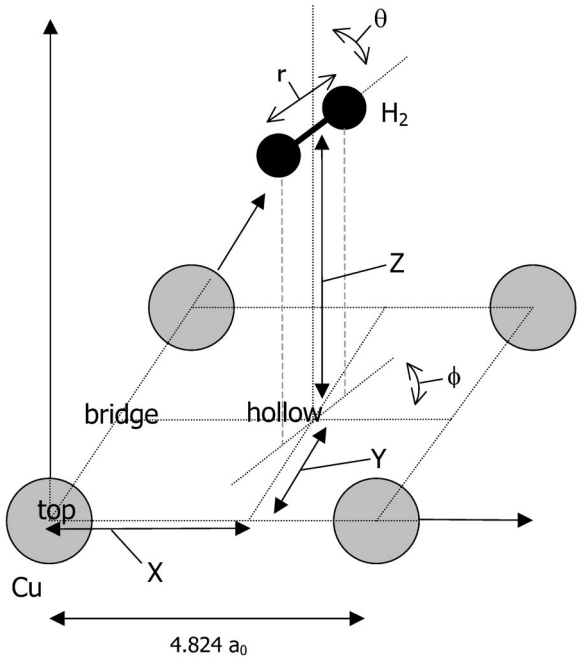

FIG. 1. Coordinate system for $H_2+Cu(100)$. Here X, Y, and Z give the position of the molecule's center-of-mass, r is the H–H distance, ϕ the azimuthal angle, and θ the polar angle of orientation of the molecule. The high-symmetry surface sites are also shown.

tions belonging to different irreducible representations. For each of these representations, a separate calculation must be performed. The number of calculations needed (one or two) and the relevant species depend on the initial value of the magnetic rotational quantum number of the molecule, m_j. Having completed the calculations for the separate irreducible representations, state-to-state probabilities for scattering and reaction probabilities can be obtained by performing a unitary transformation of the blocked symmetry-adapted scattering matrix.[68,73]

Within the SAWP method, the wave packet at time t for species Γ of the C_{4v} point group is represented as an expansion of real symmetry-adapted basis functions χ, dependent on X, Y, θ, and ϕ for species Γ.[29,30,38] A grid representation is used for the r and Z degrees of freedom,

$$\Psi^{\Gamma}_{6D}(Z_i,r_j,X,Y,\theta,\phi;t)=\sum_l f^{\Gamma}_l(Z_i,r_j;t)\chi^{\Gamma}_l(X,Y,\theta,\phi), \tag{2}$$

with l being a collective index for the quantum numbers j and m_j associated with the rotational state and n and m associated with the diffractional state of the molecule.

The initial symmetry-adapted wave packet for species Γ is propagated in time using the absorbing boundary condition (ABC)[88] evolution operator,

$$\exp(-i\hat{H}t)=\sum_{n=0}(2-\delta_{n0})\exp(-i\overline{H}t)(-i)^n J_n(\Delta H t)\hat{Q}_n, \tag{3}$$

with $\overline{H}$ and ΔH being estimates of the midpoint and half-width of the spectrum of $\hat{H}$. The J_n are Bessel functions and the $\hat{Q}_n$ are modified Chebyshev polynomials.[88] The ABC propagator incorporates the use of an optical potential to absorb the wave packets at the edges of the grid.[88]

The initial symmetry-adapted wave packets are chosen to be real and of the form of superimposed Gaussians in Z. The two Gaussian components of the initial wave packet describe a wave packet going towards the surface and its complex conjugate which moves away from the surface.[31] This choice of form of the initial wave packet and the use of the ABC propagator allows the use of real algebra throughout the propagation part of the calculations.

From the propagated wave packet, the column of the symmetry-adapted S matrix that corresponds to the initial state of the system for which the calculation was performed is obtained by projecting the wave packet onto the symmetry-adapted asymptotic gas-phase wave functions and using the scattering amplitude formalism.[68,73,89,90] After obtaining the scattering information for each symmetry species Γ, the desired column of the nonsymmetry-adapted scattering matrix can be computed.

C. Site-specific reaction probabilities

To obtain site-specific reaction probabilities, a flux-based method was used. From the time dependence of the wave packet, the stationary scattering state $\Phi(E_{\mathrm{tot}})$ and its derivative with respect to the bond length r can be computed:[91,92]

$$\Phi(E_{\mathrm{tot}})=\frac{|k_z|}{2\pi M b(-k_z)}\int_0^{\infty} e^{iE_{\mathrm{tot}}t}\Psi(t)dt, \tag{4}$$

$$\frac{\partial\Phi(E_{\mathrm{tot}})}{\partial r}=\frac{|k_z|}{2\pi M b(-k_z)}\int_0^{\infty} e^{iE_{\mathrm{tot}}t}\frac{\partial\Psi(t)}{\partial r}dt. \tag{5}$$

In these formulas k_z is the momentum conjugate to Z and $b(k_z)$ is the momentum representation conjugate to Z of the initial wave packet:

$$b(-k_z)=\frac{1}{\sqrt{2\pi}}\int_{-\infty}^{\infty}\Psi(Z;t=0)e^{ik_z t}dt. \tag{6}$$

With these three formulas, the flux through a surface at $r=r_{\mathrm{cut}}$ can be calculated as a function of the total energy for an initial state (v,j,m_j) (Ref. 92):

$$\rho(E_{\mathrm{tot}};v,j,m_j;Z,X,Y,\theta,\phi)=\frac{2\pi M}{|k_z|\mu}\mathrm{Im}\left(\Phi^*(E_{\mathrm{tot}})\frac{\partial\Phi(E_{\mathrm{tot}})}{\partial r}\bigg|_{r=r_{\mathrm{cut}}}\right). \tag{7}$$

If the flux ρ is integrated over the coordinates X, Y, Z, θ, and ϕ for a large enough value of r, the reaction probability is obtained.[91–94] However, if the flux is only integrated over Z, θ, and ϕ and the surface is positioned at a value r_{cut} which is just behind the barrier, a measure of the site reactivity can be obtained as a function of X and Y for a specific energy E_{tot}:

$$P_r(E_{\mathrm{tot}};v,j,m_j;X,Y)=\int\int\int\rho(E_{\mathrm{tot}};v,j,m_j;Z,X,Y,\theta,\phi)dZ\,d\cos(\theta)d\phi. \tag{8}$$

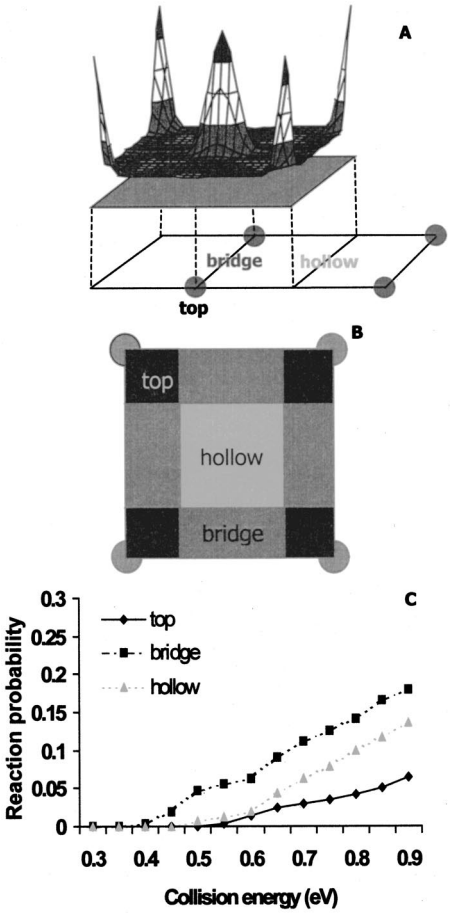

FIG. 2. (A) Example of the reaction probability density as a function of position X and Y as obtained for a specific incidence energy (0.45 eV) for H_2 ($v=0, j=2, m_j=0$). (B) The designated areas of the surface unit cell over which the reaction probability densities are integrated to obtain site-specific reaction probabilities. (C) After integration, site-specific reaction probabilities are obtained as a function of the incidence energy, for the high-symmetry bridge, top and hollow sites.

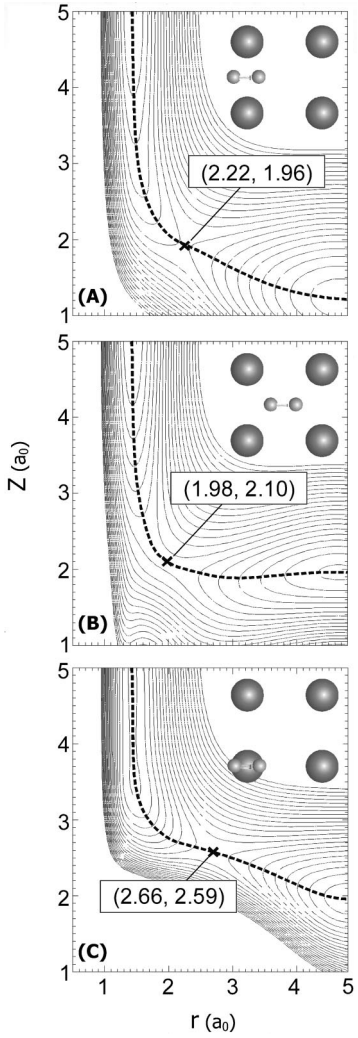

FIG. 3. $H_2+Cu(100)$ PES. Two-dimensional cuts are shown for three different reaction routes: (A) bridge-to-hollow dissociation, (B) hollow-to-bridge dissociation, and (C) top-to-bridge dissociation. The dotted line represents the reaction path and $\times$ marks the barrier location. In each case, H_2 is oriented parallel to the surface.

The function $P_r(E_{\text{tot}};v,j,m_j;X,Y)$ can be integrated over areas of the surface unit cell that have been preassigned to the high-symmetry sites on the basis of proximity (see Fig. 2) to obtain site-specific reaction probabilities $P_r^{\text{site}}(E;v,j,m_j)$. A more detailed description of the application of the flux method in the computation of site-specific reaction probabilities within the SAWP method has been given elsewhere.[26]

III. POTENTIAL ENERGY SURFACE

The 6D PES used in this study is based on 14 two-dimensional cuts in the coordinates r and Z with the H_2 placed on the high-symmetry sites. For each of these cuts, points were calculated with DFT,[76,77] using the generalized gradient approximation[95–97] (GGA) and a slab representation of the metal surface. In the representation of the Cu surface, the experimental Cu(100) bulk lattice constant ($\alpha_{\text{lat}} = 4.824a_0$) has been used. The convergence of the DFT calculations is believed to be within 0.1 eV of the GGA limit of this system. Details on the DFT calculations for these 2D PES can be found in Ref. 26.

The full 6D PES, known as PES IV,[26] is expanded in 14 symmetry-adapted functions of X, Y, θ, and ϕ. In the expansion, the r,Z-dependent expansion coefficients are related to the computed 2D cuts by the inversion of a set of linear equations.[26]

In Fig. 3 the most essential aspects of the $H_2+Cu(100)$ PES are shown. The lowest barrier (0.50 eV) corresponds to dissociation above the bridge site with the H atoms moving towards the hollow sites and H_2 oriented parallel to the surface. The highest minimum barrier found above a high-symmetry site corresponds to H_2, oriented parallel to the surface, dissociating above the top site with the H atoms moving towards the bridge sites (0.63 eV). In Table I, barrier heights found at the high-symmetry sites are collected for different azimuthal angles and for H_2 oriented parallel to the surface.

In Table II, barrier locations and two measures of the anisotropy are shown for the high-symmetry sites. The polar anisotropy is defined by the range of potentials experienced by H_2 when located at the minimum barrier and rotated out of plane, keeping all of the other degrees of freedom fixed. The azimuthal anisotropy is defined by rotating the molecule

TABLE I. Listed are barrier heights for different orientations and surface sites. The labels A, B, and C correspond to the labels used in Fig. 3.

Surface site	θ	ϕ	Barrier in eV
Bridge (A)	90	0	0.50
Bridge	90	45	0.84
Bridge	90	90	1.19
Top (C)	90	0	0.63
Top	90	45	0.73
Hollow (B)	90	0	0.58
Hollow	90	45	0.65

parallel to the surface and keeping all the other degrees of freedom fixed at the minimum barrier geometry of a high-symmetry site.

The top-site barrier is the ''latest'' and shows the largest polar anisotropy (12.92 eV), whereas the largest azimuthal anisotropy is found for the bridge site (2.39 eV). The hollow and top sites both show a weak azimuthal anisotropy at the corresponding barrier geometry's, 0.05 and 0.09 eV, respectively. The site with the lowest polar anisotropy is the hollow site, which displays the earliest barrier of all the high-symmetry sites considered.

IV. COMPUTATIONAL DETAILS

Calculations have been performed for all initial states of H_2 with $(v=0, j=0-5)$ and with $(v=1, j=0-5)$. The calculations for the $(v=0)$ states have been performed for the incidence energy range of 0.3–0.9 eV. The $(v=1)$ state calculations have been performed for two incidence energy ranges, one from 0.1 to 0.3 eV and one from 0.2 to 0.65 eV, using a smaller rotational basis set for the lower-energy range. The overlapping region of incidence energy (0.2–0.3 eV) has been used to confirm convergence of both calculations of the $(v=1)$ states. [Note that for initially $(v=1, j=1, m_j=1)$ H_2, no site-specific reaction probabilities have been calculated for the energy range 0.1–0.2 eV.] In all the calculations the initial wave packet was propagated for 60 000 a.u. of time.

In all calculations, the diffractional basis employed all functions with $|n|+|m|\leqslant 11$. For the odd-j states, the rotational basis included functions with $j\leqslant 29$, and for the even-j states, $j\leqslant 28$ was used for all of the $(v=0)$ calculations and the $(v=1)$ calculations for the higher-incidence-energy range. The rotational basis $j\leqslant 20$ has been used for the $(v=1)$, even-j-valued initial states in the 0.1–0.3 eV incidence energy range. For the odd-j-valued $(v=1)$ initial states, $j\leqslant 19$ has been used for the lower-energy range. All other parameters have not been changed with respect to earlier studies.[26,31] Tests conducted indicated convergence of reaction and scattering probabilities to within 1% with respect to basis sizes and propagation time.

TABLE II. Listed here are the heights and locations of the minimum barriers of the high symmetry sites. Also listed are the two measures of the potential anisotropy found at these sites (see the text).

	Bridge (A)	Hollow (B)	Top (C)
Barrier height in eV	0.50	0.58	0.63
Barrier position r in a_0	2.22	1.98	2.66
Barrier position Z in a_0	1.96	2.10	2.59
ϕ anisotropy in eV	2.39	0.05	0.09
θ anisotropy in eV	1.42	0.56	12.92

V. RESULTS AND DISCUSSION

A. Degeneracy-averaged reaction probabilities

In Fig. 4 degeneracy-averaged reaction probabilities $P_{\mathrm{deg}}(E;v,j)$ are shown for $(v=0, j=0-5)$ and $(v=1, j=0-5)$. These $P_{\mathrm{deg}}(E;v,j)$ have been calculated from the initial-state-resolved reaction probabilities $P_r(E;v,j,m_j)$ using

$$P_{\mathrm{deg}}(E;v,j)=\frac{1}{2j+1}\sum_{m_j=0}^{m_j=j}(2-\delta_{m_j0})P_r(E;v,j,m_j). \quad (9)$$

The molecules incident in the vibrationally excited $(v=1)$ state [Fig. 4(B)] react at much lower energies than molecules initially in the vibrational ground state $(v=0)$ [Fig. 4(A)] an effect called vibrational enhancement.[36,46,51] Here we focus on the dependence of reaction on the rotational quantum level j of the incident molecule. A striking difference between $(v=0)$ and $(v=1)$ is that, at low incidence energies where the reaction probability is low (near the reaction threshold), the $P_{\mathrm{deg}}(E;v,j)$ clearly increases with j for $(v=1)$ (rotational enhancement), whereas $P_{\mathrm{deg}}(E;v,j)$ is almost independent of j for $(v=0)$.

Such behavior has not been observed in experimental studies on the analogous systems $D_2(v=0,1,2)+\mathrm{Cu}(111)$ (Refs. 3 and 4) and $H_2(v=0,1)+\mathrm{Cu}(111)$ (Ref. 12). In the fits to the experimentally measured associative-desorption probabilities for Cu(111), $P_{\mathrm{deg}}(E;v,j)$ first decreases with j for $j=0$ up to about 5 (rotational hindering) and then increases with j (rotational enhancement) for both $(v=0)$ and $(v=1)$. The explanation offered for rotational hindering is that rotating molecules are less likely to pass the entire barrier region in an orientation that remains favorable for reaction.[3,4,12,33,39,48] Rotational enhancement can be explained by the presence of a late barrier: at the barrier, the rotational constant of the molecule is lower than in the gas phase, allowing conversion of energy from rotation to motion along the reaction path, thereby helping the molecule to overcome the barrier.[3,4,33,48] The higher j, the stronger this effect; eventually, this dominates the hindering effect.

To explain the difference in the dependence of $P_{\mathrm{deg}}(E;v,j)$ on j between $(v=0)$ and $(v=1)$ for $H_2+\mathrm{Cu}(100)$ near threshold and the difference with the experimental results for $H_2, D_2+\mathrm{Cu}(111)$, we will first consider where on the surface unit cell the molecule dissociates for $(v=0)$ and $(v=1)$. Next, we will discuss how the degeneracy-averaged site-specific reaction probabilities $P^{\mathrm{site}}_{\mathrm{deg}}(E;v,j)$ depend on j for both the $(v=0)$ and $(v=1)$ molecules. We will show that the j dependence of $P^{\mathrm{site}}_{\mathrm{deg}}(E;v,j)$ can be explained on the basis of previous fixed-site[25,39] and flat-surface[44,48] calculations, by relating the computed j dependence to the anisotropy of the PES at different sites. We end this section by showing how experimental measurement of the j dependence of $P_{\mathrm{deg}}(E;v,j)$

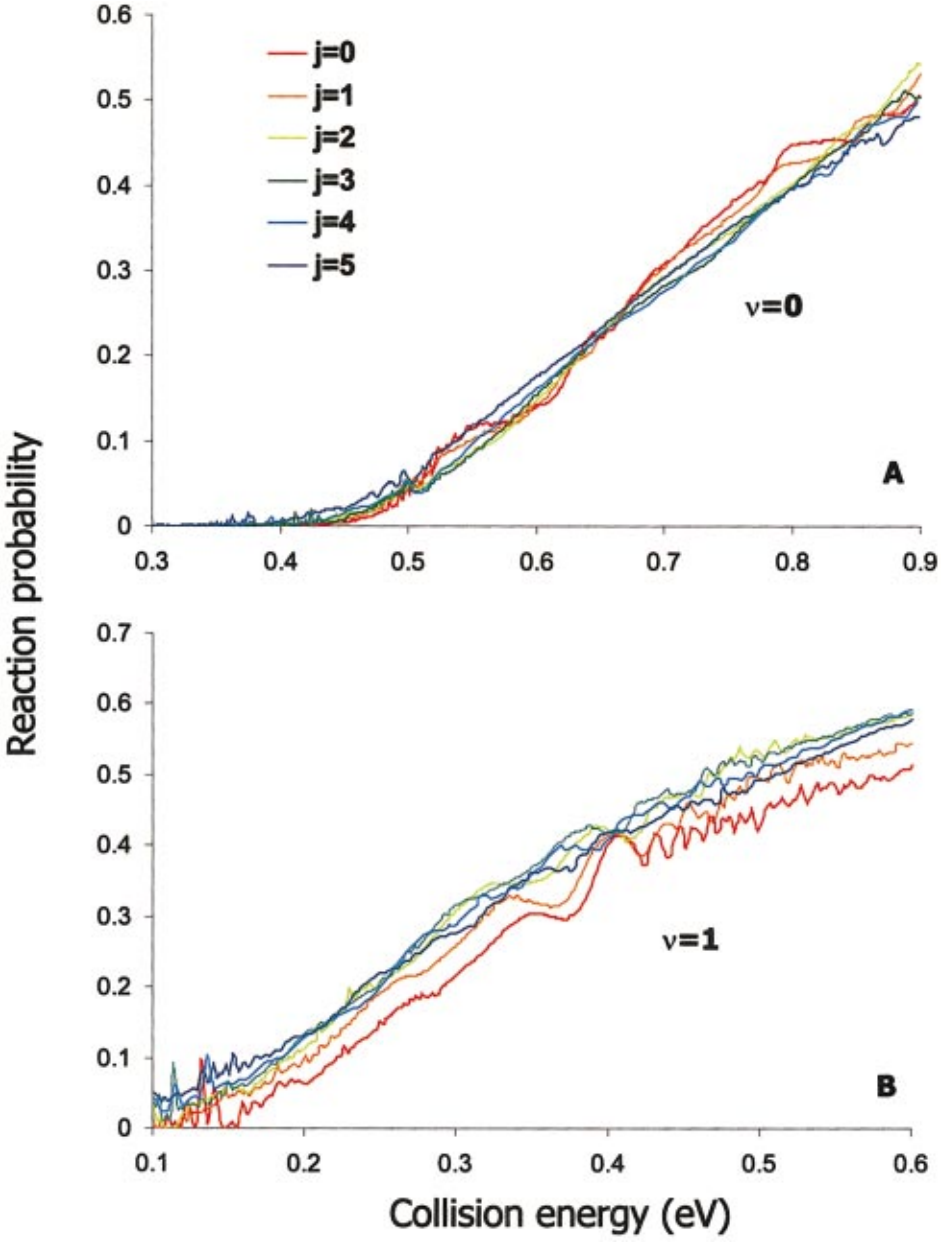

FIG. 4. (Color) Degeneracy-averaged reaction probability as a function of normal incidence energy, for different rotational states j, for $(v=0)$ (A) and $(v=1)$ (B) H_2.

might confirm our predictions concerning the preferred reaction site of $H_2(v=0)$ and $H_2(v=1)$ on Cu(100).

The results of a previous study[26,27] showed that for the $(v=0, j=0)$ and $(v=0, j=4)$ states, the reaction takes place predominantly at the bridge site. The $(v=1, j=0)$ and the $(v=1, j=4)$ states, however, react preferably at the top site at near threshold incidence energies. In Figs. 5 and 6 the degeneracy-averaged site-specific reaction probabilities $[P_{\mathrm{deg}}^{\mathrm{site}}(E;v,j)]$ are shown for the states $(v=0, j=1-3,5)$ and $(v=1, j=1-3,5)$, respectively. The $P_{\mathrm{deg}}^{\mathrm{site}}(E;v,j)$ have been calculated from the $P_r^{\mathrm{site}}(E;v,j,m_j)$ using an expression analogous to Eq. (9). Figures 5 and 6 clearly show that the previous theoretical result—that, on Cu(100), $(v=0)$ H_2 preferentially reacts at the bridge site, whereas $(v=1)$ H_2 preferentially reacts at the top site for incidence energies just above threshold—is general for low initial j $(j=0-5)$.

As explained before,[26,27] $(v=0)$ H_2 preferentially reacts at the bridge site because the barrier to reaction is lowest at this site (see Table II). At relatively low energies, $(v=1)$ H_2 reacts preferentially at the top site because H_2 can convert all of its vibrational energy (in excess of the zero-point vibrational energy) to energy of motion along the reaction path to overcome the higher barrier at this site. This is possible due to the special features of the top-site PES, which has a reaction path with an especially late barrier (see Table II) and a high curvature in front of the barrier [see Fig. 3(C)].[26,27,98]

It is worthwhile to consider whether the different j dependences of $P_{\mathrm{deg}}(E;v,j)$ of $(v=0)$ and $(v=1)$ H_2 at energies just above threshold (Fig. 4) can be explained from the differences in the preferred reaction site of these vibrational states (Figs. 5 and 6). For this purpose, $P_{\mathrm{deg}}^{\mathrm{site}}(E;v,j)$ for $(j=0-5)$ are plotted separately for each site, for both $(v=0)$ (Fig. 7) and $(v=1)$ (Fig. 8). Just above the threshold, the reaction at the top site shows clear rotational enhance-

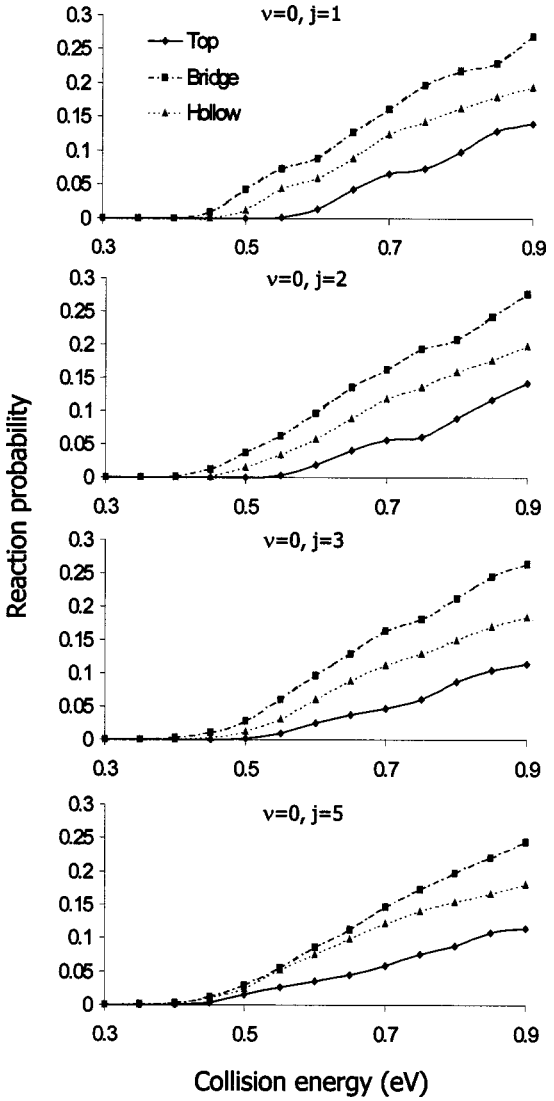

FIG. 5. Site-specific degeneracy-averaged reaction probability for the ($v=0$) state as a function of the incidence energy for specific rotational levels.

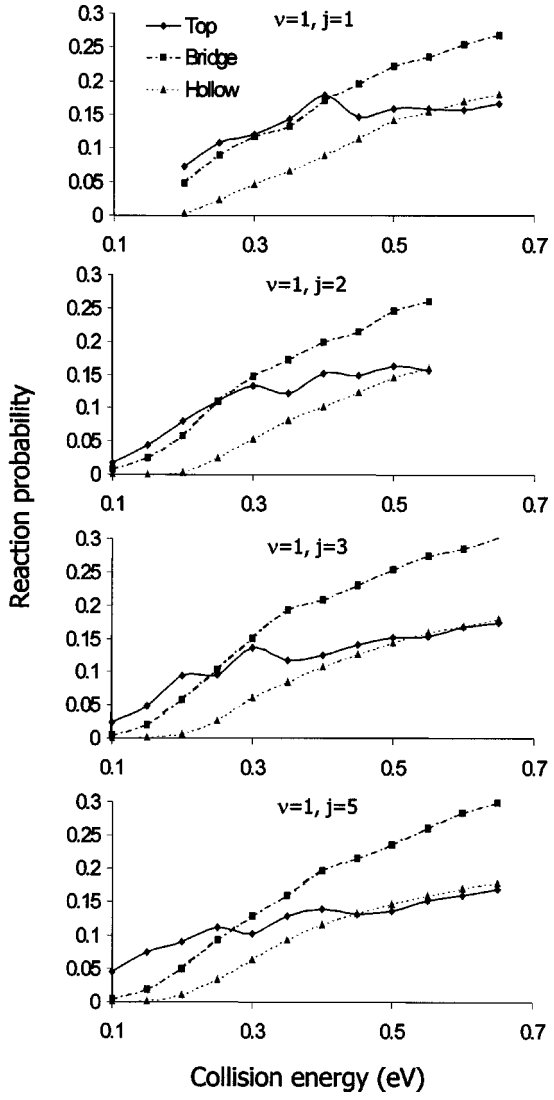

FIG. 6. Site-specific degeneracy-averaged reaction probability for the ($v=1$) state as a function of the incidence energy for specific rotational levels.

ment, not just for ($v=1$) [as in $P_{\mathrm{deg}}(E;v,j)$, Fig. 4(B)], but also for ($v=0$). In contrast, the reaction above the bridge site appears to be almost independent of j, not just for ($v=0$) [as in $P_{\mathrm{deg}}(E;v,j)$, Fig. 4(A)], but also for ($v=1$).

The difference in the j dependence of the reaction between the bridge and top sites can be explained by differences in the topology of the PES at these sites. The barrier at the top site shows little azimuthal anisotropy (see Table II). Previous reduced dimensionality studies of H_2+Cu which employed the flat-surface approximation—so that the potential contains no azimuthal anisotropy—also showed the reaction to be rotationally enhanced for low j for energies just above the threshold.[44,48] Similar results were obtained in fixed-site studies of H_2+Cu for sites at which the potential has little azimuthal anisotropy at the reaction barrier geometry [see, for example, Fig. 7 of Ref. 39 for the reaction above the top site of Cu(111) and Fig. 9 of Ref. 25 for the reaction above the hollow site for Cu(100)]. The reason for this trend is that helicoptering molecules, which have $|m_j|=j$ and are the ones first to react just above threshold,[13,29,33,35,48] can react without (or with little) rotational hindering in the absence of (a large) azimuthal anisotropy. The reaction will then be rotationally enhanced due to the lateness of the barrier, which leads to a reduction of the molecule's rotational constant at the barrier. In Figs. 7 and 8, the reaction at the hollow site is less rotationally enhanced than the reaction at the top site because the barrier is earlier at the hollow site (see Table II).

In flat-surface calculations modeling the dissociation of H_2 on Cu(111), Darling and Holloway showed that they could recover the experimentally found trend that the reaction is rotationally hindered for low j (Refs. 3 and 4) by introducing azimuthal anisotropy in their potential.[48] Employing a fixed-site LEPS potential based on DFT calculations,[79] Dai and Zhang likewise recovered the experimental trend that the reaction is hindered in calculations for the reaction on the lowest barrier bridge site, above which the barrier has a high azimuthal anisotropy.[39] Similarly, we find that reaction above the bridge site of Cu(100) is not rotationally enhanced at low j. The reason, again, is that the potential barrier has a high azimuthal anisotropy above the bridge site

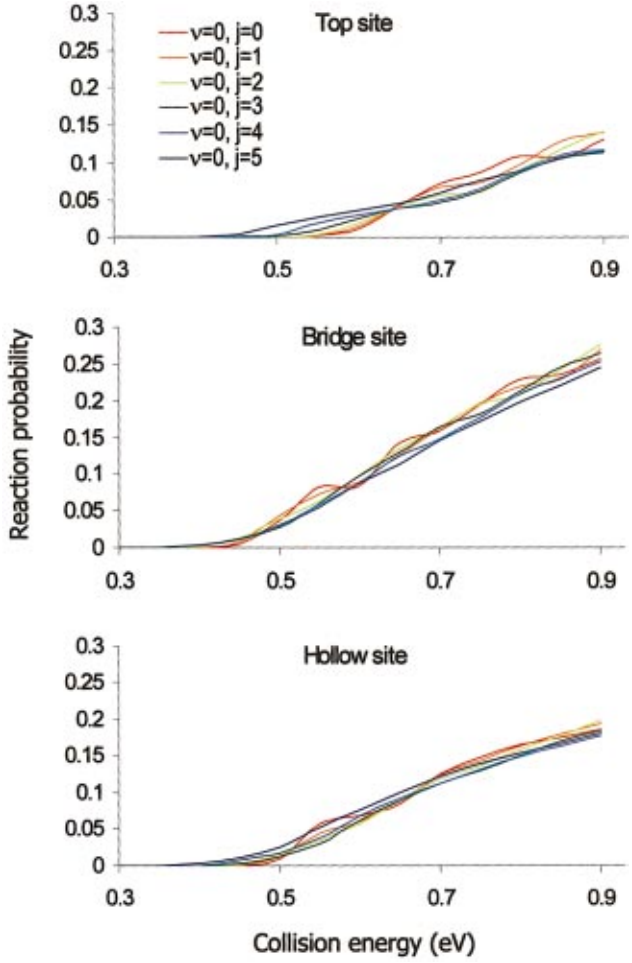

FIG. 7. (Color) Site-specific degeneracy-averaged reaction probability as a function of the incidence energy for different rotational levels of the ($v=0$) state. These spline curves were based on the same data points shown in Fig. 5.

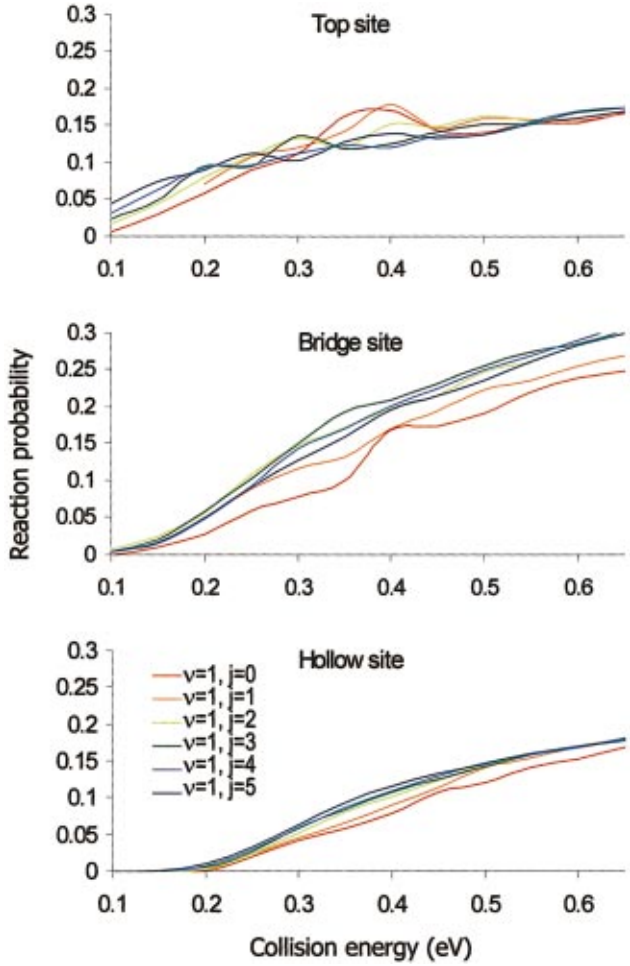

FIG. 8. (Color) Site-specific degeneracy-averaged reaction probability as a function of the incidence energy for different rotational levels of the ($v=1$) state. These spline curves were based on the same data points shown in Fig. 6.

(see Table II), so that the rotational motion also hinders the reaction of helicoptering molecules. For Cu(100), this compensates the enhancement effect due to the late barrier, so that no clear dependence of the reaction on j is found. The increased lateness of the barrier at the top site also contributes to the rotational enhancement of the reaction of ($v=1$) $H_2+Cu(100)$ in addition to the absence of azimuthal anisotropy discussed above.

Our 6D calculations predict reaction of H_2 on Cu(100) to be nearly independent of j for ($v=0$) and to be clearly rotationally enhanced for ($v=1$) at low j and incidence energies. This result differs from experimental[3,4,12] and theoretical[33] ($v=0$) results for $H_2, D_2+Cu(111)$, which show a net rotational hindering effect for low j. This difference could be due to a difference in the location of the minimum reaction barrier for Cu(100) and Cu(111). On Cu(100), the barrier occurs at a value of the H–H distance, which is 0.1 Å larger than on Cu(111).[99] Therefore, rotational enhancement should be more important for Cu(100) and is here predicted to offset rotational hindering for ($v=0$) and to dominate for ($v=1$). This prediction can be easily tested by performing energy-resolved associative-desorption experiments in which the desorbing H_2 is detected state selectively with respect to v and j, as have already been performed for $H_2, D_2+Cu(111)$.[12,20]

The associative-desorption experiments we propose are usually done using high surface temperatures T_s ($T_s \geqslant 370$ K),[86,87] whereas our calculations are done for a 0-K surface. However, increasing T_s is not expected to change the j dependence of the reaction probability at low collision energies. It is known from associative desorption experiments that, for H_2 and D_2 on Cu(111), the dependence of the sticking probability on the surface temperature can be modeled easily by assigning larger width parameters to the fitted, S-shaped reaction probability curves when considering higher surface temperatures.[86,87] Furthermore, for ($v=0$) H_2 and D_2 the increase of the width with T_s was found to be independent of j.[86] If we assume the same to be true for ($v=0,1$) $H_2+Cu(100)$, the effect of increasing T_s would be to increase all $P_{deg}(E;v,j)$ by a similar amount for low E. Then $P_{deg}(E;v,j)$ would still be approximately independent of j for $v=0$ and increase with j for $v=1$.

Our most important result is that, just above threshold, the site-specific degeneracy-averaged reaction probability increases with j for the top site and is nearly independent of j above the bridge site. Because this difference can also be

explained by differences in the topology of the PES at these sites, we predict that the j dependence of the total reaction probability, which is an experimentally measurable quantity, can be used as a signature for the preferred reaction site. Confirmation of our prediction of no j dependence of reaction for $(v=0)$ and rotational enhancement for $(v=1)$ would strongly support our finding that $(v=0)$ and $(v=1)$ H_2 react at different sites on Cu(100), i.e., on the bridge and top sites, respectively.

B. Experimental signatures based on the comparison of alignments

The rotational quadrupole alignment $A_0^{(2)}(E;v,j)$ of the molecules that react can be calculated from initial state (v,j,m_j) resolved reaction probabilities using the following expression:[100]

$$A_0^{(2)}(E;v,j)=\frac{\Sigma_{m_j}P_r(E;v,j,m_j)(\{3m_j^2/j(j+1)\}-1)}{\Sigma_{m_j}P_r(E;v,j,m_j)}. \tag{10}$$

Here $A_0^{(2)}(E;v,j)$ is a quantity revealing information on the $|m_j|$ distribution of molecules, initially in level (v,j), which go on to react. The maximum value of the alignment for a given j level, $3j/(j+1)-1$, corresponds to the situation where only helicoptering molecules react $(|m_j|=j)$. The minimum value, -1.0, corresponds to the situation where only cartwheeling molecules react $(m_j=0)$ and an alignment of zero corresponds to helicoptering and cartwheeling molecules reacting with equal probability.[26] Assuming the validity of detailed balance, desorption probabilities, as measured in associative desorption experiments, are equal to reaction probabilities, as measured in adsorption experiments, for desorption normal to the surface. Therefore $A_0^{(2)}(E;v,j)$ is an experimentally measurable quantity.[13]

In a previous study,[26] it was noted that $A_0^{(2)}(E;v=1,j=4)$ is higher than $A_0^{(2)}(E;v=0,j=4)$ for near threshold incidence energies. It was suggested that this behavior could be correlated to the reaction taking place predominantly at the top site for $(v=1)$ H_2 and at the bridge site for $(v=0)$ H_2. Here we address the question of whether this signature for the difference in reaction site between $(v=0)$ and $(v=1)$ H_2 is also valid for the j levels 1–3 and 5.

In Fig. 9, $A_0^{(2)}(E;v,j)$ is plotted as a function of *shifted* incidence energies. The energies have been shifted to an offset corresponding to a total reaction probability of 5%, for which we know the reaction will take place at either the top site (for $v=1$) or the bridge site (for $v=0$), to enable a better comparison between reaction of H_2 in these two initial vibrational levels.

Clearly, at or just above the energy offset, reacting $(v=1,j=2)$ and $(v=1,j=3)$ H_2 do not have a higher $A_0^{(2)}(E;v,j)$ than $(v=0,j=2)$ and $(v=0,j=3)$ H_2, respectively (Fig. 9). In particular, close to threshold, $A_0^{(2)}(E;v=0,j=2)$ is even higher than $A_0^{(2)}(E;v=1,j=2)$. For $(v=1,j=4)$ and $(v=1,j=5)$ H_2 has a higher $A_0^{(2)}(E;v,j)$ than $(v=0)$ H_2 for $j=4$ and 5 at incidence energies slightly larger than the energy offset. The $(j=1)$ level shows a behavior similar to that of the $(j=4)$ and $(j=5)$ levels, with the exception that both $A_0^{(2)}(E;v=1,j=1)$ and $A_0^{(2)}(E;v=0,j=1)$ have reached their maximum value of 0.5 at the energy offset. In previous publications,[26,27] $A_0^{(2)}(E;v=1,j=4)$ was plotted significantly higher than $A_0^{(2)}(E;v=0,j=4)$ at the energy offset. This was due to an error in the program used to compute the alignments.[82] Here we present the correct plots.

Figure 9 clearly shows that the result previously obtained for $(j=4)$—that $A_0^{(2)}(E;v,j)$ is higher for $(v=1)$ somewhat above the energy for which the reaction probability exceeds 5%—is not general for low j. The explanation offered for the greater alignment of $(j=4)$ reacting molecules, for $(v=1)$ compared to $(v=0)$, was based on steric hindering.[26] Vibrationally excited H_2 reacts preferentially at the top site. At the barrier of this site, the anisotropy in θ is higher than at the bridge site barrier, where $(v=0)$ H_2 prefers to react. This by itself should lead to a greater preference for the helicopter reaction at the top site. In addition, the reaction of helicoptering H_2 can proceed almost without rotational hindering at the top site, due to the low potential anisotropy in ϕ at this site's barrier. In contrast, the reaction at the bridge site, which exhibits a strong ϕ anisotropy, should be rotationally hindered for helicopters (see Table II). These two factors were the key elements in the explanation of the difference between the alignments of $(v=0)$ and $(v=1)$ for $(j=4)$ H_2 at and slightly beyond threshold.

However, this reasoning predicts that $A_0^{(2)}(E;v=1,j)$ should also be higher than $A_0^{(2)}(E;v=0,j)$ also for $j=1-3$ and $j=5$, for incidence energies at and slightly beyond threshold, because the top site is the preferred reaction site for $(v=1)$ H_2 and the bridge site for $(v=0)$ H_2. As already stated, $A_0^{(2)}(E;v=1,j)$ is not always higher than $A_0^{(2)}(E;v=0,j)$, especially at the energy offset (Fig. 9). An explanation for this can be found by not only considering the steric hindering effects, but by also including rotational enhancement effects into the picture, as will be discussed below.

The steric hindering effects, mentioned above, can be divided into two separate mechanisms.[26] The first is *orientational hindering* and the second *rotational hindering*. Rotational hindering originates from the fact that molecules rotating fast enough may encounter an unfavorable orientation while travelling along the reaction path, regardless of the initial orientation of the molecule. If a high anisotropy is present in the neighborhood of the barrier, this may of course lead to reflection. In contrast, orientational hindering refers to a static effect: Nonrotating or slow-rotating molecules will be reflected from an anisotropic barrier if their initial orientation is unfavorable for a reaction.

Rotation may hinder the reaction, but it can also help molecules to react. Rotational enhancement effects can also occur by two different mechanisms. In the first mechanism, rotation enhances the reaction due to the decrease of the molecule's rotational constant as it approaches a late barrier.[36] For this mechanism, which will be called *elastic rotational enhancement*, the higher the j level is, the more rotational energy can be transferred into motion along the reaction path. Elastic rotational enhancement will enhance cartwheels and helicopters, of a given j level, equally well, and it should therefore have a less direct influence on the

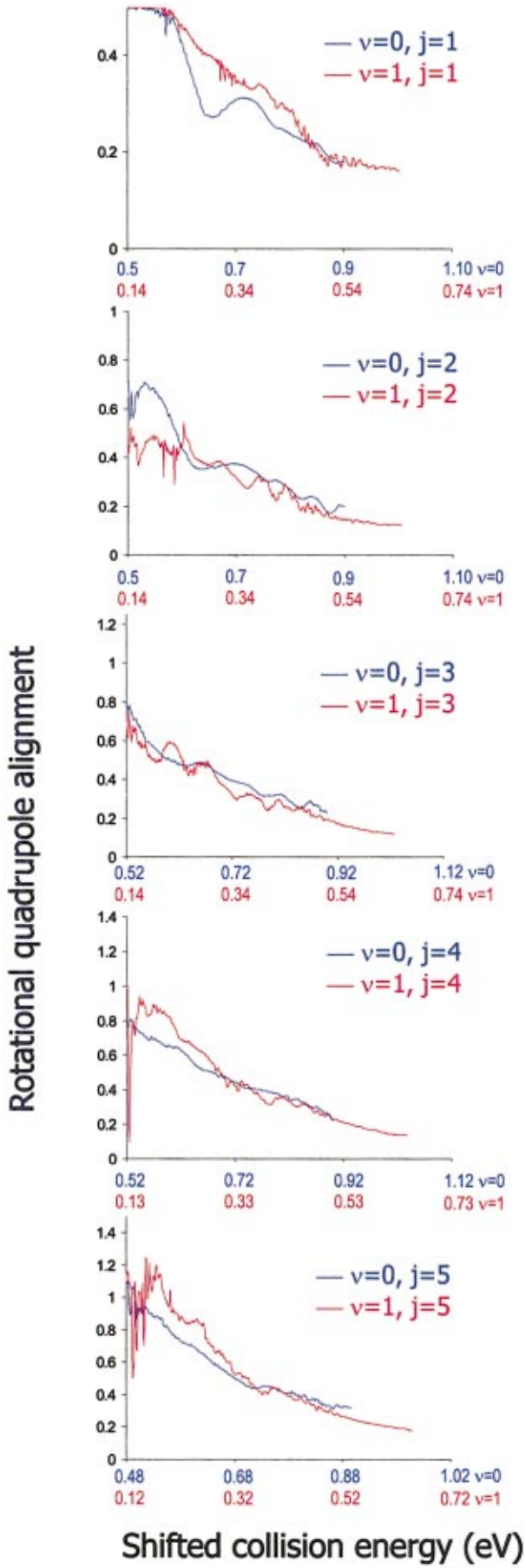

FIG. 9. (Color) Comparison of the rotational quadrupole alignment of reacting (v,j) molecules is shown between the $(v=0)$ and $(v=1)$ states for different rotational levels. The energy scales have been shifted to an offset for which the total reaction probability is 5% for each (v,j) state.

rotational quadrupole alignment of the reacting molecules. [Equation (10) shows that increasing $P_r(E;v,j,m_j)$ for all mj should lead to a lowering of the absolute value of the alignment.]

The second mechanism of enhancement is closely related to the potential anisotropy (in θ) near the barrier. Not only will a high anisotropy induce hindering effects, as explained above, it may also allow the molecule to *rotationally deexcite* on its way to the barrier and thereby help the reaction. The energy gained from this deexcitation can be transferred into motion along the reaction path and thereby help the molecule to cross the barrier.[101] Due to the inversion symmetry of H_2, this mechanism can only be effective for molecules with $j \geqslant 2$. In addition, we will show that its effectiveness is very dependent on the specific (j,m_j) level of H_2. This mechanism of rotational enhancement is referred to as *inelastic rotational enhancement*. It is expected to be especially important near threshold, where reaction may only be possible through this mechanism.

Having identified these four mechanisms (which are summarized in Table III and are further discussed below), the observed j dependence of the relative $(v=0)$ and $(v=1)$ H_2 rotational quadrupole alignments can now be understood. For the $(j=1)$ case, both $A_0^{(2)}(E;v=1,j=1)$ and $A_0^{(2)}(E;v=0,j=1)$ reach the value of 0.5 at the energy offset. This corresponds to *only* helicopters being reactive. The $(j=1)$ helicopters are oriented favorably for reactions on both the bridge $(v=0\ H_2)$ and the top site $(v=1\ H_2)$ compared to the $(j=1)$ cartwheels. At slightly higher incidence energies the $(j=1)$ cartwheels will start to react as well, so both $A_0^{(2)}(E;v=1,j=1)$ and $A_0^{(2)}(E;v=0,j=1)$ will decrease with energy.

However, $A_0^{(2)}(E;v=0,j=1)$ will decrease more rapidly than $A_0^{(2)}(E;v=1,j=1)$ due to the fact that the higher θ anisotropy of the top site induces a greater *orientational hindering* of the reaction of the $v=1$ cartwheels compared to the $v=0$ cartwheels reacting at the bridge site. On top of that, the $(v=0)$ helicopters experience more rotational hindering due to the ϕ anisotropy of the reaction barrier being higher at the $(v=0)$ H_2 reaction site (bridge) than at the $(v=1)$ H_2 reaction site (top). The effects of rotational enhancement on the alignment of the reacting molecules can be ruled out for the $(j=1)$ case. No rotational deexcitations are possible because for H_2 the change in j must be even and the energy released by elastic rotational enhancement, although present, is believed to have no direct influence on the alignment.

This changes when considering the differences between the $(v=0)$ and $(v=1)$ H_2 rotational quadrupole alignments for $(j=2)$ incident molecules. $A_0^{(2)}(E;v=0,j=2)$ is higher than $A_0^{(2)}(E;v=1,j=2)$ at the energy offset. Based on hindering arguments alone, this cannot be understood, because $(v=1)$ H_2 reacts preferably at the top site and $(v=0)$ H_2 at the bridge site. The top site, having the most anisotropy in θ and the least anisotropy in ϕ, should give rise to a greater preference for the helicopter reaction than the bridge site. The explanation can be found by considering the inelastic rotational enhancement mechanism.

For $(v=1,j=2)$ H_2 reacting at the top site, considerable

TABLE III. Mechanisms that affect the reaction probabilities and the rotational quadrupole alignment of reacting molecules. Also presented are the features in the PES which are the most relevant to the mechanism, the surface site for which the mechanism is most important, the effect each mechanism has on the reaction probability, and the rotational quadrupole alignment for the different rotational states of the incident H_2 molecule.

	Mechanism	PES feature responsible	Site(s) at which most important	Effect on reaction near threshold	Effect on $A_0^{(2)}(E;v,j)$
Enhancement mechanisms	Elastic rotational enhancement	Small rotational constant at a late barrier	Most important at top site	$P_{deg}(E;v,j)$ increases with j	none
	Inelastic rotational enhancement	θ anisotropy of the PES at barrier	Most important at top site	$P_r(E;v,j,m_j)$ is enhanced for low $\lvert m_j\rvert$ and $j \geqslant 2$	$A_0^{(2)}(E;v,j)$ decreases
Steric hindering mechanisms	Orientational hindering	θ anisotropy of the PES at barrier	Most important at top site	$P_r(E;v,j,m_j)$ is reduced for small $\lvert m_j\rvert$	$A_0^{(2)}(E;v,j)$ increases
	Rotational hindering	Anisotropy of the PES at barrier	Bridge site (ϕ) top site (θ)	$P_{deg}(E;v,j)$ decreases with j	$A_0^{(2)}(E;v,j)$ increases with θ anisotropy and decreases with ϕ anisotropy

θ anisotropy exists, which not only leads to hindering, but also enables H_2 to deexcite into the $(v=1, j=0)$ state before dissociating [or into the librational state that corresponds adiabatically[102] to the $(v=1, j=0)$ state]. Because the top site shows a nearly isotropic barrier in ϕ, m_j will be almost conserved[42,43] in collisions with the top site. The only possible rotational deexcitation from the $(v=1, j=2)$ level of H_2, with $\Delta j=2$ and $\Delta m_j=0$, is the $(v=1, j=2, m_j=0) \rightarrow (v=1, j=0, m_j=0)$ transition. The energy released through the rotationally inelastic mechanism will therefore mostly enhance the reaction of the $(j=2)$ cartwheels, resulting in a decreased alignment of the reacting $(j=2)$ molecules. Here $(v=0)$ H_2, which reacts at the bridge site, encounters less anisotropy in θ. It is therefore believed that inelastic rotational enhancement is more important for $(v=1)$ H_2 than it is for $(v=0)$ H_2. The greater increase of reactivity of $(v=1, j=2, m_j=0)$ H_2 is expected to lower the rotational quadrupole alignment of reacting $(v=1, j=2)$ H_2 more than for $(v=0, j=2)$ H_2, as is seen in Fig. 9 for energies close to the energy offset.

Support for the importance of rotationally inelastic enhancement of the reaction of $(v=1, j=2)$ cartwheels comes from Fig. 10. In this figure the m_j-resolved reaction probabilities for $(v=1, j=2)$ and $(v=0, j=2)$ H_2 are shown as a function of the incidence energy. The effect of the sudden allowance of $(v=1, j=2, m_j=0) \rightarrow (v=1, j=0, m_j=0)$ deexcitation near threshold energies is clear. Apparently, energy released by the $(v=1, j=2, m_j=0) \rightarrow (v=1, j=0, m_j=0)$ H_2 deexcitation enhances the reaction of $(v=1, j=2, m_j=0)$ H_2 considerably compared to $(v=0, j=2, m_j=0)$ H_2 [the reaction probability of the $(v=1, j=2)$ cartwheel is almost as large as that of the $(v=1, j=2)$ helicopter, and this is clearly not the case for $(v=0, j=2)$ H_2]. Based on steric arguments, we would instead expect the cartwheel reaction to be much less effective for $(v=1)$ H_2, which reacts at the site with the greater θ anisotropy.

Additional support can be found in the state-to-state scattering probabilities of H_2 from different initial $j=2$ states. In Fig. 11 the absolute scattering probabilities $P(v, j=2, m_j \rightarrow v, j=0)$ are shown for $(v=0)$ and $(v=1)$, for $(m_j=0)$ and $(m_j=2)$ (transitions with $\Delta m_j=1$ are forbidden for the PES used[26]). Again, in this figure, the energy scale has been shifted to an offset where the total reaction probability is 5% for each initial vibrational state. Clearly, at the energy offset, the initial $(v=1, j=2, m_j=0)$ H_2 shows a higher probability for vibrationally elastic and rotationally inelastic scattering into the $(j=0)$ state than the initial $(v=0, j=2, m_j=0)$ H_2. This suggests a higher probability for rotational deexcitation for the molecule on its way to the barrier, and this would also be expected to lead to greater enhancement of the $(v=1)$ reaction of cartwheels near threshold through the rotationally inelastic enhancement mechanism discussed above. On the other hand, the initial

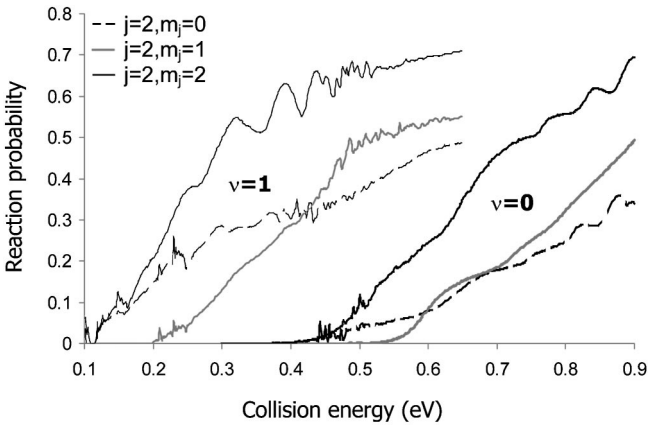

FIG. 10. Initial-state (v, j, m_j) resolved reaction probabilities are shown vs normal incidence energy for $(v, j=2, m_j)$ H_2 for ($v=0$ and 1 and $m_j=0-2$).

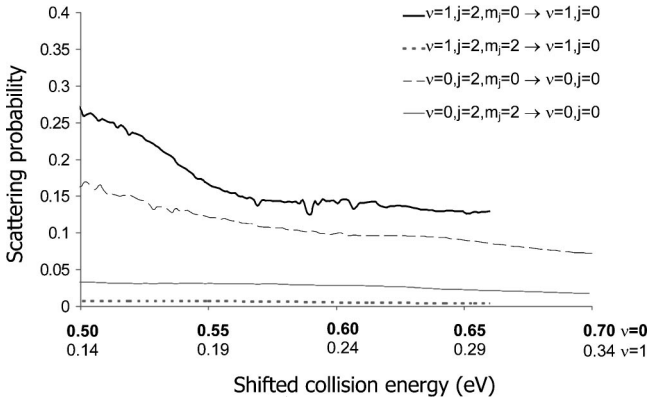

FIG. 11. Probability for rotational deexcitation, $P(v,j=2,m_j \rightarrow v, j=0)$, is shown for $v=0$ and 1 and $m_j=0$ and 2. The $(v=0)$ and $(v=1)$ energy scales have been shifted to an offset corresponding to the energy for which $(v,j=2)$ H_2 shows a degeneracy-averaged reaction probability of 5%.

$(v=1,j=2,m_j=2)$ H_2 shows nearly no inelastic scattering into the $(v=1,j=0)$ state. The rotational deexcitation probabilities for $(v=1,j=2)$ cartwheels (high) and helicopters (low) are consistent with scattering from a site with a high θ anisotropy and a low ϕ anisotropy—i.e., the top site (see Table II). Furthermore, the initial $(v=0,j=2,m_j=2)$ H_2 shows a higher probability of rotationally inelastic scattering into the $(j=0)$ state than initial $(v=1,j=2,m_j=2)$ H_2. This is consistent with $(v=0,j=2,m_j=2)$ H_2 scattering from a site with a higher ϕ anisotropy—i.e., the bridge site (see Table II). It is clear that rotational deexcitation and the reaction near threshold are intimately related processes, which occur at similar sites. These processes are related through the anisotropy of the potential at the barrier associated with the reaction site. As a result, the rotationally inelastic scattering results can be used to help identify reaction sites and to make inferences regarding the reaction mechanisms.

For $(v=1,j=2)$ H_2, the mechanism of inelastic rotational enhancement is clearly present. A similar reasoning can be applied to the comparison between $A_0^{(2)}(E;v=0,j=3,4,5)$ and $A_0^{(2)}(E;v=1,j=3,4,5)$ at the energy offset. For these j levels several transitions with $\Delta j=2$ and $\Delta m_j=0$ are allowed. For $(v=1,j=3)$ H_2, both $(m_j=1)$ and $(m_j=0)$ are allowed to deexcite into $(v=1,j=1,m_j=1)$ and $(v=1,j=1,m_j=0)$, respectively. For $(v=1,j=4)$ and $(v=1,j=5)$ even more transitions are possible, causing the lowering of the alignment, resulting from enhancement of the nonhelicopter state reaction, to be less dramatic. On top of that, the energy gap associated with these transitions increases with increasing j. The associated energy gap for the transition $(v=1,j=3) \rightarrow (v=1,j=1)$ H_2 ($\approx$0.068 eV) is much larger than that for the transition $(v=1,j=2) \rightarrow (v=1,j=0)$ H_2 ($\approx$0.041 eV) making the inelastic rotational enhancement for $(j=3)$ H_2 less probable. It is therefore believed that the importance of inelastic rotational enhancement decreases with increasing j. For $(j=4)$ and $(j=5)$, the inelastic enhancement effect is expected only to be visible at the energy offset, if at all. Beyond the energy offset, steric hindering becomes the dominating factor in determining the ratio of $(v=1)$ H_2 alignment and $(v=0)$ H_2 alignment. For the reaction of $(j=4)$ and $(j=5)$ H_2, orientational and rotational hinderings are expected to be most important, for both the reaction of initial $(v=0)$ and $(v=1)$ H_2. Both hindering mechanisms will ensure that, beyond the energy offset, $A_0^{(2)}(E;v=1,j=4,5)$ will be higher than $A_0^{(2)}(E;v=0,j=4,5)$. The $(j=3)$ H_2 case can, in this picture, be regarded as the intermediate case, in which the inelastic rotational enhancement and hindering effects on the reaction cancel in the influence exerted on the alignment of the reacting molecules. The above explanation accounts for all the trends seen in Fig. 9.

For $j>1$ H_2, the rotational quadrupole alignments do not reach their maximum limiting values at the energy offset. Previous calculations on $H_2+Cu(100)$ (Ref. 35) and $H_2+Cu(111)$ (Ref. 33) showed a downturn of the alignment of the reacting molecules at low collision energies. It is not completely clear whether the effect that the alignment does not reach its maximum limiting value can be completely attributed to the rotationally inelastic enhancement mechanism. As noted before, we expect this mechanism to become less important for high j, because the energy gap associated with rotational deexcitation increases with initial j. It is possible that the effect is partly due to steering (m_j scrambling) becoming important at low collision energies.[53] Finally, it should be noted that the quantum-mechanical cartwheel states also have a finite probability of being oriented exactly parallel (j is even) or almost parallel (any j) to the surface. In a picture in which rotation is not considered to take place in a ''classical'' sense, this may still lead to a reaction of those cartwheel molecules which happen to be in the right ''window of orientation'' when they get to the barrier and this may also contribute to the lowering of the alignment of reacting molecules for higher j near threshold energies.

Despite the fact that the experimental signature of $A_0^{(2)}(E;v=1,j) > A_0^{(2)}(E;v=0,j)$, at and beyond the energy offset, is not as general as one might hope,[26] the difference between $A_0^{(2)}(E;v=1,j)$ and $A_0^{(2)}(E;v=0,j)$, for $j=1$, 4, and 5, can still be used to identify top-site reactivity through experimental measurement. The mechanisms causing the differences between $A_0^{(2)}(E;v=1,j)$ and $A_0^{(2)}(E;v=0,j)$, somewhat above threshold, can be related to specific features of the PES at both the top and bridge sites. Specifically, for $j=1$, 4, and 5, $A_0^{(2)}(E;v=1,j)$ is expected to be higher than $A_0^{(2)}(E;v=0,j)$ at energies slightly beyond threshold and this difference is clearly related to the top-site reactivity of $(v=1)$ H_2: the reaction barrier at the top site has a greater θ anisotropy, causing more orientational hindering of the cartwheel reaction. Measurement of this would confirm our prediction of the difference in preferred reaction site between $(v=0)$ and $(v=1)$ H_2 on Cu(100), whereas the measurement of $A_0^{(2)}(E;v=1,j=2)$ being lower than $A_0^{(2)}(E;v=0,j=2)$, together with a high inelastic scattering probability, $P(v=1,j=2\ H_2 \rightarrow v=1,j=0)$, of H_2 at threshold energies, would not only confirm the top-site reactivity, but also the importance of inelastic rotational enhancement for the reaction of $(v=1,j=2,m_j=0)$ incident H_2.

The differences we predict between $A_0^{(2)}(E;v=0,j)$ and $A_0^{(2)}(E;v=1,j)$ can be confirmed experimentally using cur-

rently available techniques, but once again the measurements would have to be performed at high T_s (approximately 900 K),[13] whereas our prediction was derived for a 0-K surface. The effect an elevated surface temperature will have on the alignment signature is not completely clear to us. As mentioned before, associative-desorption experiments on D_2 and $H_2+Cu(111)$ (Ref. 86) suggest that the width of the S-shaped degeneracy-averaged reaction probability curves $P_{deg}(E;v,j)$ will increase with T_s for H_2 on Cu(100). One might expect the same to be true for the $P_r(E;v,j,m_j)$. If, at low E, the $P_r(E;v,j,m_j)$ were to increase by the same amount for all m_j, application of Eq. (10) would lead to a lower value of the alignment. However, the midpoint of the S-shaped reaction probability curve generally shifts to higher E with decreasing $|m_j|$ and the saturation value of the reaction probability decreases with decreasing $|m_j|$ (see, for instance, Fig. 3 of Ref. 35). This suggests that, at low E, the temperature-induced broadening of the reaction probability curve would increase $P_r(E;v,j,m_j)$ more for large $|m_j|$ than for small $|m_j|$ and that the measured alignment could be more or less independent of T_s. We therefore expect that the requirement of a high T_s in the experiment should not really hamper the experimental confirmation of our predictions regarding alignment.

VI. SUMMARY

In this study we have calculated initial-state-resolved reaction probabilities for $H_2+Cu(100)$, for the $(v=0, j=0-5)$ and the $(v=1, j=0-5)$ states of H_2, for normal incidence only, modeling the motion in all six degrees of freedom of H_2. In the quantum dynamical calculations, the symmetry-adapted wave packet method[31] was used. The ground-state potential energy surface used in this study (PES IV) was taken from density functional theory calculations, with the Cu(100) surface being represented by a slab with application of periodic boundary conditions and using the generalized gradient approximation.[26] We used the recently implemented flux analysis method to obtain initial-state-selective site-specific reaction probabilities for the bridge, hollow, and top sites.[26]

Analysis of the site-specific degeneracy-averaged reaction probabilities showed that, for all j levels studied, the initial $(v=1)\,H_2$ prefers to react at the top site and initial $(v=0)\,H_2$ at the bridge site, near threshold energies. The mechanism behind the greater reactivity of $(v=1)\,H_2$ at the top site derives from special features of the PES at the top site, i.e., a reaction path with a large curvature in front of an especially late barrier.[26,27,98] Initially vibrationally excited H_2 molecules can be vibrationally deexcited on the way to the barrier, converting their excess vibrational energy into energy of motion along the reaction path, thus reacting at low incidence energies better at the top site. For the initial $(v=0)\,H_2$ molecules, the preferred reaction site could be understood solely on the basis of the relative barrier heights [the $(v=0)\,H_2$ reaction site has the lowest barrier to reaction].

Site-specific degeneracy-averaged reaction probabilities also showed that, in general, the lateness of the top-site barrier induces a clear elastic rotational enhancement effect: rotational energy can be used to overcome the barrier because the rotational constant is lowered at the barrier, due to the H-H distance being longer. For reaction at the top site, this was found to be the case for both initial $(v=1)\,H_2$ and initial $(v=0)\,H_2$. The absence of azimuthal anisotropy at the top-site barrier also plays a large role, allowing molecules in helicopter states to react without rotational hindering above that site. The bridge site, having an earlier barrier, which is more anisotropic in ϕ than the top-site barrier, showed no such behavior. This finding was related to other theoretical studies of reduced dimensionality on the same or similar systems. Because initial $(v=1)\,H_2$ tends to react at the top site at near threshold energies, the total reaction probabilities show a clear elastic rotational enhancement near threshold for $(v=1)\,H_2$. This, by itself, is a signature for top site reaction of $v=1\,H_2$ that could be measured in associative desorption experiments. On the other hand, near threshold the reaction of $(v=0)\,H_2$ shows no rotational enhancement because it reacts at the bridge site. If experimentally measured reaction probabilities would show a clear elastic rotational enhancement effect near threshold for initial $(v=1)\,H_2$ and not for $(v=0)\,H_2$, this would strongly support our theoretical finding that $(v=1)\,H_2$ reacts at the top site and $(v=0)\,H_2$ at the lowest barrier bridge site.

The dependence of the reaction of $(v=0)$ and $(v=1)\,H_2$ on j that is here predicted for Cu(100) [no dependence for $(v=0)$, rotational enhancement at low j for $(v=1)$] differs from that measured for $H_2+Cu(111)$.[12] Specifically, on Cu(111) the reaction of H_2 is hindered for low j and rotationally enhanced for $j>4$, for both $(v=0)$ and $(v=1)$. The difference between the j dependence of the reaction of H_2 on Cu(100) and Cu(111) was attributed to differences in barrier locations, reaction barriers being later for the Cu(100) surface.

A detailed analysis of the previously found experimental signature,[26,27] based on the comparison of the $(v=0)$ and $(v=1)$ rotational quadrupole alignments of reacting H_2, has been presented for all j levels considered. The observed trends could not be explained by steric hindering arguments alone, as was possible for initial $(j=4)\,H_2$. These arguments are only sufficient to explain the alignment of initial $j=1$, 4, and 5 reacting H_2. The alignment of reacting $(j=2)$ and $(j=3)\,H_2$ is also strongly affected by inelastic rotational enhancement near threshold energies. Near threshold, a mechanism in which the molecule converts its rotational energy into energy in motion along the reaction path may be the only mechanism through which it can react. For $(v=1)\,H_2$, which reacts at a site (top) which has a very large polar anisotropy, the rotational deexcitation mechanism is especially effective for cartwheel states, lowering the alignment of reacting H_2 near threshold. The inelastic rotational enhancement mechanism is most effective for $(j=2)$ and $(j=3)\,H_2$ because rotational deexcitation may occur with small energy gaps for these low-j levels.

All observed trends in the relative heights of the rotational quadrupole alignments of $(v=1)$ and $(v=0)$ reacting H_2 molecules close to threshold have been shown to correlate to specific features of the PES at the preferred reaction site. This makes the measurement of the relative alignments

of $(v=0)$ and $(v=1)$ reacting molecules suitable for identifying the reaction site, although the interpretation is more complicated than could have been anticipated from previous results for $(j=4)\,H_2$ only. Specifically, if the rotational quadrupole alignment of initial $(v=1, j=1, 4,$ and $5)\,H_2$ is measured to be higher than the rotational quadrupole alignment of initial $(v=0, j=1, 4,$ and $5)\,H_2$ at energies close to threshold, this indicates that $(v=1)\,H_2$ reacts at the top site and $(v=0)\,H_2$ at the bridge site. If at the same time the rotational quadrupole alignment of reacting $(v=1, j=2)$ molecules were measured to be lower than for $(v=0, j=2)$ near threshold, this would support our finding that the reaction of $(j=2)$ cartwheels can be enhanced through a rotationally inelastic mechanism. It would also give further support to our theoretical finding that $(v=1)\,H_2$ reacts at the top site and $(v=0)\,H_2$ at the bridge site.

Our predictions can be confirmed in experiments using currently available techniques, provided that detailed balance holds so that reaction probabilities can be inferred from associative desorption probabilities. Specifically, the rotational enhancement signature can be confirmed in associative desorption experiments using time-of-flight techniques and laser detection (for instance, resonantly enhanced multiphonon ionization) to obtain reaction (desorption) probabilities that are resolved with respect to the collision (desorption) energy and the (v,j) level of H_2.[12] The rotational quadrupole alignment of reacting (desorbing) H_2 can be measured by performing two different experiments with linearly polarized laser light, taking the polarization normal to the surface in the one experiment and parallel in the other.[13] Confirmation of our predictions for Cu(100) would add significant weight to our belief in the predicting power of present-day functionals (based on the generalized gradient approximation) of DFT: it would show that DFT can predict the location of the lowest reaction barrier, as well as relative barrier heights and detailed features of the potential at barrier geometries that determine the reactivities for specific initial (v,j,m_j) states of H_2.

ACKNOWLEDGMENTS

The National Computing Facilities foundation (NCF), VUA beta-cluster, part of the Distributed ASCI Supercomputer and the Research School Combination ''Catalysis Controlled by Chemical Design'' (NRSC-Catalysis) are hereby acknowledged for their financial support. Also, the Office of Naval Research is thanked for the financing of the work done at the NRL. The research of M.F.S. was supported by CW/NWO through an open competition grant.

[1] G. R. Darling and S. Holloway, Rep. Prog. Phys. **58**, 1595 (1995).
[2] B. E. Hayden, in *Dynamics of Gas-Surface Interactions*, edited by C. T. Rettner and M. N. R. Ashfold (The Royal Society of Chemistry, Letchworth, 1991), pp. 137–170.
[3] H. A. Michelsen, C. T. Rettner, and D. J. Auerbach, Phys. Rev. Lett. **69**, 2678 (1992).
[4] H. A. Michelsen, C. T. Rettner, D. J. Auerbach, and R. N. Zare, J. Chem. Phys. **98**, 8294 (1993).
[5] L. Schröter, R. David, and H. Zacharias, J. Vac. Sci. Technol. A **9**, 1712 (1991).
[6] M. Gostein and G. P. Sitz, J. Chem. Phys. **106**, 7378 (1997).
[7] B. E. Hayden and C. L. A. Lamont, Phys. Rev. Lett. **63**, 1823 (1989).
[8] L. Schröter, H. Zacharias, and R. David, Phys. Rev. Lett. **62**, 571 (1989).
[9] G. D. Kubiak, G. O. Sitz, and R. N. Zare, J. Chem. Phys. **83**, 2538 (1985).
[10] L. Schröter, R. David, and H. Zacharias, Surf. Sci. **258**, 259 (1991).
[11] K. D. Rendulic and A. Winkler, Surf. Sci. **299–300**, 261 (1994).
[12] C. T. Rettner, H. A. Michelsen, and D. J. Auerbach, J. Chem. Phys. **102**, 4625 (1995).
[13] H. Hou, S. J. Gulding, C. T. Rettner, A. M. Wodtke, and D. J. Auerbach, Science **277**, 80 (1997).
[14] D. Wetzig, R. Dopheide, M. Rutkowski, R. David, and H. Zacharias, Phys. Rev. Lett. **76**, 463 (1996).
[15] D. Wetzig, M. Rutkowski, R. David, and H. Zacharias, Europhys. Lett. **36**, 31 (1996).
[16] S. J. Gulding, A. M. Wodtke, H. Hou, C. T. Rettner, H. A. Michelsen, and D. J. Auerbach, J. Chem. Phys. **105**, 9702 (1996).
[17] M. Gostein, H. Parhikhteh, and G. O. Sitz, Phys. Rev. Lett. **75**, 342 (1995).
[18] A. Hodgson, P. Samson, A. Wights, and C. Cottrell, Phys. Rev. Lett. **78**, 963 (1997).
[19] A. Hodgson, J. Moryl, P. Traversaro, and H. Zhao, Nature (London) **356**, 501 (1992).
[20] C. T. Rettner, D. J. Auerbach, and H. A. Michelsen, Phys. Rev. Lett. **68**, 2547 (1992).
[21] G. Anger, A. Winkler, and K. D. Rendulic, Surf. Sci. **220**, 1 (1989).
[22] G. Comsa and R. David, Surf. Sci. **117**, 77 (1982).
[23] H. A. Michelsen and D. J. Auerbach, J. Chem. Phys. **94**, 7502 (1991).
[24] E. Watts, G. O. Sitz, D. A. McCormack, G. J. Kroes, R. A. Olsen, J. A. Groeneveld, J. N. P. v. Stralen, E. J. Baerends, and R. C. Mowrey, J. Chem. Phys. **114**, 495 (2001).
[25] R. C. Mowrey, G. J. Kroes, and E. J. Baerends, J. Chem. Phys. **108**, 6906 (1998).
[26] D. A. McCormack, G. J. Kroes, R. A. Olsen, J. A. Groeneveld, J. N. P. v. Stralen, E. J. Baerends, and R. C. Mowrey, Faraday Discuss. **117**, 109 (2000).
[27] D. A. McCormack, G. J. Kroes, R. A. Olsen, J. A. Groeneveld, J. N. P. v. Stralen, E. J. Baerends, and R. C. Mowrey, Chem. Phys. Lett. **328**, 317 (2000).
[28] G. J. Kroes, E. J. Baerends, and R. C. Mowrey, Phys. Rev. Lett. **78**, 3583 (1997).
[29] D. A. McCormack, G. J. Kroes, E. J. Baerends, and R. C. Mowrey, Faraday Discuss. **110**, 267 (1998).
[30] D. A. McCormack, G. J. Kroes, R. A. Olsen, E. J. Baerends, and R. C. Mowrey, Phys. Rev. Lett. **82**, 1410 (1999).
[31] G. J. Kroes, E. J. Baerends, and R. C. Mowrey, J. Chem. Phys. **107**, 3309 (1997).
[32] J. Q. Dai and J. C. Light, J. Chem. Phys. **107**, 1676 (1997).
[33] J. Q. Dai and J. C. Light, J. Chem. Phys. **108**, 7816 (1998).
[34] R. C. Mowrey, G. J. Kroes, G. Wiesenekker, and E. J. Baerends, J. Chem. Phys. **106**, 4248 (1997).
[35] D. A. McCormack, G. J. Kroes, R. A. Olsen, E. J. Baerends, and R. C. Mowrey, J. Chem. Phys. **110**, 7008 (1999).
[36] D. Halstead and S. Holloway, J. Chem. Phys. **93**, 2859 (1990).
[37] J. Q. Dai and J. Z. H. Zhang, Surf. Sci. **319**, 193 (1994).
[38] G. J. Kroes, G. Wiesenekker, E. J. Baerends, and R. C. Mowrey, Phys. Rev. B **53**, 10397 (1996).
[39] J. Q. Dai and J. Z. H. Zhang, J. Chem. Phys. **102**, 6280 (1995).
[40] J. Harris, Surf. Sci. **221**, 335 (1989).
[41] G. R. Darling and S. Holloway, Surf. Sci. **268**, 1305 (1992).
[42] J. Sheng and J. Z. H. Zhang, J. Chem. Phys. **97**, 6784 (1992).
[43] J. Sheng and J. Z. H. Zhang, J. Chem. Phys. **99**, 1373 (1993).
[44] J. Q. Dai, J. Sheng, and J. Z. H. Zhang, J. Chem. Phys. **101**, 1555 (1994).
[45] G. R. Darling and S. Holloway, Faraday Discuss. **110**, 253 (1998).
[46] M. R. Hand and S. Holloway, J. Chem. Phys. **91**, 7209 (1989).
[47] G. R. Darling and S. Holloway, Surf. Sci. **304**, L461 (1994).
[48] G. R. Darling and S. Holloway, J. Chem. Phys. **101**, 3268 (1994).
[49] G. R. Darling, M. Kay, and S. Holloway, Surf. Sci. **400**, 314 (1998).
[50] T. Burner and W. Brenig, Surf. Sci. **317**, 303 (1994).
[51] G. R. Darling and S. Holloway, Surf. Sci. **307–409**, 153 (1994).
[52] M. Hand and S. Holloway, Surf. Sci. **211**, 940 (1989).
[53] G. J. Kroes, Prog. Surf. Sci. **60**, 1 (1999).
[54] R. C. Mowrey, J. Chem. Phys. **99**, 7049 (1993).
[55] G. R. Darling and S. Holloway, Faraday Discuss. **96**, 43 (1993).
[56] G. J. Kroes, G. Wiesenekker, E. J. Baerends, R. C. Mowrey, and D. Neuhauser, J. Chem. Phys. **105**, 5979 (1996).
[57] G. R. Darling and S. Holloway, Chem. Phys. Lett. **191**, 396 (1992).

[58] G. R. Darling and S. Holloway, J. Chem. Phys. **97**, 5182 (1992).
[59] D. Wetzig, M. Rutkowski, H. Zacharias, and A. Gross, Phys. Rev. B **63**, 205412 (2000).
[60] A. Gross and M. Scheffler, Chem. Phys. Lett. **263**, 567 (1996).
[61] A. Gross and M. Scheffler, Phys. Rev. Lett. **77**, 405 (1996).
[62] A. Gross, S. Wilke, and M. Scheffler, Surf. Sci. **358**, 614 (1996).
[63] A. Gross and M. Scheffler, Phys. Rev. B **57**, 2493 (1998).
[64] A. Gross, C. M. Wei, and M. Scheffler, Surf. Sci. **416**, L1095 (1998).
[65] A. Gross and M. Scheffler, Prog. Surf. Sci. **53**, 187 (1996).
[66] A. Gross and M. Scheffler, Chem. Phys. Lett. **256**, 417 (1996).
[67] A. Gross, S. Wilke, and M. Scheffler, Phys. Rev. Lett. **75**, 2718 (1995).
[68] G. J. Kroes, J. G. Snijders, and R. C. Mowrey, J. Chem. Phys. **102**, 5512 (1994).
[69] G. R. Darling and S. Holloway, J. Electron Spectrosc. Relat. Phenom. **64–65**, 517 (1993).
[70] H. F. Busnengo, W. Dong, and A. Salin, Chem. Phys. Lett. **320**, 328 (2000).
[71] H. F. Busnengo, C. Crespos, W. Dong, A. Salin, and J. C. Rayez, Phys. Rev. B **63**, 041402 (2001).
[72] A. Gross, J. Chem. Phys. **110**, 8696 (1999).
[73] G. J. Kroes, J. G. Snijders, and R. C. Mowrey, J. Chem. Phys. **103**, 5121 (1995).
[74] C. Engdahl, B. I. Lundqvist, U. Nielsen, and J. K. Nørskov, Phys. Rev. B **45**, 11362 (1992).
[75] C. Engdahl and U. Nielsen, J. Chem. Phys. **98**, 4223 (1993).
[76] P. Hohenberg and W. Kohn, Phys. Rev. B **136**, B864 (1964).
[77] W. Kohn and L. J. Sham, Phys. Rev. A **140**, A1133 (1965).
[78] G. Wiesenekker, G. J. Kroes, and E. J. Baerends, J. Chem. Phys. **104**, 7344 (1996).
[79] B. Hammer, M. Scheffler, K. W. Jacobsen, and J. K. Nørskov, Phys. Rev. Lett. **73**, 1400 (1994).
[80] S. Wilke and M. Scheffler, Phys. Rev. B **53**, 4926 (1996).
[81] A. Eichler, J. Hafner, A. Gross, and M. Scheffler, Phys. Rev. B **59**, 13297 (1999).
[82] D. A. McCormack, G. J. Kroes, R. A. Olsen, J. A. Groeneveld, J. N. P. v. Stralen, E. J. Baerends, and R. C. Mowrey, Chem. Phys. Lett. **346**, 347 (2001).
[83] G. J. Kroes, A. Gross, E. J. Baerends, M. Scheffler, and D. A. McCormack, Acc. Chem. Res. **35**, 193 (2002).
[84] A. Gross, Surf. Sci. Rep. **32**, 291 (1998).
[85] M. Dohle and P. Saalfrank, Surf. Sci. **373**, 95 (1997).
[86] M. J. Murphy and A. Hodgson, J. Chem. Phys. **108**, 4199 (1998).
[87] H. A. Michelsen, C. T. Rettner, and D. J. Auerbach, Surf. Sci. **272**, 65 (1992).
[88] V. A. Mandelshtam and H. S. Taylor, J. Chem. Phys. **103**, 2903 (1995).
[89] G. G. Balint-Kurti, R. N. Dixon, and C. C. Marston, Int. Rev. Phys. Chem. **11**, 317 (1992).
[90] G. G. Balint-Kurti, R. N. Dixon, and C. C. Marston, J. Chem. Soc. **86**, 1741 (1990).
[91] A. Messiah, *Quantum Mechanics* (Wiley, New York, 1958).
[92] R. A. Olsen, P. H. T. Philipsen, E. J. Baerends, G. J. Kroes, and O. M. Lovvik, J. Chem. Phys. **106**, 9286 (1997).
[93] D. H. Neuhauser, M. Baer, R. S. Judson, and D. J. Kouri, Comput. Phys. Commun. **63**, 460 (1991).
[94] D. H. Zhang and J. Z. H. Zhang, J. Chem. Phys. **101**, 1146 (1994).
[95] J. P. Perdew, Phys. Rev. B **33**, 8822 (1986).
[96] S. H. Vosko, L. Wilk, and M. Nusair, Can. J. Phys. **58**, 1200 (1980).
[97] A. D. Becke, Phys. Rev. A **38**, 3098 (1988).
[98] G. R. Darling and S. Holloway, J. Chem. Phys. **97**, 734 (1992).
[99] P. Kratzer, B. Hammer, and J. K. Nørskov, Surf. Sci. **359**, 45 (1996).
[100] R. N. Zare, *Angular momentum* (Wiley-Interscience, New York, 1988), pp. 226–242.
[101] W. A. Dino, H. Kasai, and A. Okiji, J. Radiol. Prot. **67**, 1571 (1998).
[102] G. R. Darling, M. Kay, and S. Holloway, Phys. Rev. Lett. **78**, 1731 (1997).